TrkB hyperactivity contributes to brain dysconnectivity, epileptogenesis, and anxiety in zebrafish model of Tuberous Sclerosis Complex

Magdalena Kedra[a], Katarzyna Banasiak[a], Katarzyna Kisielewska[a], Lidia Wolinska-Niziol[a], Jacek Jaworski[a,1], and Justyna Zmorzynska[a,1]

[a]Laboratory of Molecular and Cellular Neurobiology, International Institute of Molecular and Cell Biology, 02-109 Warsaw, Poland

Edited by Lawrence Steinman, Stanford University School of Medicine, Stanford, CA, and approved December 16, 2019 (received for review June 29, 2019)

Tuberous Sclerosis Complex (TSC) is a rare genetic disease that manifests with early symptoms, including cortical malformations, childhood epilepsy, and TSC-associated neuropsychiatric disorders (TANDs). Cortical malformations arise during embryonic development and have been linked to childhood epilepsy before, but the underlying mechanisms of this relationship remain insufficiently understood. Zebrafish have emerged as a convenient model to study elementary neurodevelopment; however, without in-depth functional analysis, the Tsc2-deficient zebrafish line cannot be used for studies of TANDs or new drug screening. In this study, we found that the lack of Tsc2 in zebrafish resulted in heterotopias and hyperactivation of the mTorC1 pathway in pallial regions, which are homologous to the mammalian cortex. We observed commissural thinning that was responsible for brain dysconnectivity, recapitulating TSC pathology in human patients. The lack of Tsc2 also delayed axonal development and caused aberrant tract fasciculation, corresponding to the abnormal expression of genes involved in axon navigation. The mutants underwent epileptogenesis that resulted in nonmotor seizures and exhibited increased anxiety-like behavior. We further mapped discrete parameters of locomotor activity to epilepsy-like and anxiety-like behaviors, which were rescued by reducing tyrosine receptor kinase B (TrkB) signaling. Moreover, in contrast to treatment with vigabatrin and rapamycin, TrkB inhibition rescued brain dysconnectivity and anxiety-like behavior. These data reveal that commissural thinning results in the aberrant regulation of anxiety, providing a mechanistic link between brain anatomy and human TANDs. Our findings also implicate TrkB signaling in the complex pathology of TSC and reveal a therapeutic target.

Tuberous Sclerosis Complex | TANDs | brain dysconnectivity | anxiety | TrkB

Tuberous Sclerosis Complex (TSC) is an autosomal dominant disorder that is caused by loss-of-function mutations in the *TSC1* or *TSC2* genes (1), the products of which form a complex that negatively regulates mechanistic/mammalian target of rapamycin (mTOR) complex 1 (mTORC1), a complex necessary for proper neuronal development (2). In TSC, epilepsy is the most prominent neurological symptom, which begins in the first year of life and often evolves into an intractable form (3). Epilepsy is accompanied by TSC-associated neuropsychiatric disorders (TANDs), including intellectual disability (ID) and anxiety (4). Epilepsy is thought to be caused by cortical malformations (5) that consist of heterotopias, tubers, and white matter (WM) dysconnectivity in TSC (4). Tubers are often diagnosed in utero, suggesting that the pathology of TSC is acquired during embryonic development (6).

Cortical malformations result in childhood epilepsy and intractable or treatment-refractory seizures in various other diseases, underscoring the importance of proper cortex development (5). The existing mammalian models of TSC mimic human disease in many aspects, including cortical malformations and seizures (7–13). However, these models present difficulties in studying TSC pathology during embryonic development in utero when cortical malformations that lead to epileptogenesis arise (14). Thus, the present study comprehensively examined brain development and behavior in zebrafish, which provide an opportunity to study early neuronal development in vivo due to external development and body transparency. Although zebrafish do not contain a cortex per se, the homologous structures are present, the majority of which are localized to the pallium (15–17).

Previous studies investigated the utility of *tsc2*^{vu242} mutant zebrafish as a model of TSC and reported abnormalities in pallial WM organization (including the disruption of WM with ectopic cell bodies), a decrease in locomotion, and abnormal brain activity in the optic tectum (18, 19). However, these studies did not elaborate potential disease mechanisms. Moreover, neurobehavioral changes that mimic symptoms of human TANDs were not investigated in *tsc2*$^{vu242/vu242}$ mutants. Therefore, in this study, we performed an in-depth analysis of changes in brain connectivity during development. We evaluated *tsc2*^{vu242} fish behavior and mapped seizure activity and anxiety-like behavior to discrete parameters of locomotion. Finally, we tested the ability of drugs to rescue TSC-associated phenotypes and found that reducing tyrosine receptor kinase B (TrkB) signaling reversed brain dysconnectivity, epileptogenesis,

Significance

Tuberous Sclerosis Complex (TSC) is a hereditary disease that presents with early brain malformations, childhood epilepsy, and TSC-associated neuropsychiatric disorders (TANDs). Cortical malformations arise in utero and have been linked to childhood epilepsy before. Externally developing zebrafish seem convenient to study elementary neurodevelopment; however, without the in-depth functional analysis, the Tsc2-deficient zebrafish cannot be used for studies of TANDs. Here, we found that Tsc2-deficient zebrafish recapitulated symptoms seen in TSC patients on anatomical and behavioral levels, including aberrant brain morphology, thinning of brain connections, epileptogenesis, and increased anxiety-like behavior, which was rescued by reducing TrkB signaling, revealing a potential drug target. Moreover, we show that commissural thinning cause aberrant regulation of anxiety, providing a link between brain anatomy and emotion.

Author contributions: J.Z. designed research; J.J. and J.Z. secured funding; M.K., K.B., K.K., L.W.-N., and J.Z. performed research; M.K. and J.Z. analyzed data; M.K, J.J., and J.Z. interpreted the data; and M.K., J.J., and J.Z. wrote the paper.

The authors declare no competing interest.

This article is a PNAS Direct Submission.

[1]To whom correspondence may be addressed. Email: jaworski@iimcb.gov.pl or jzmorzynska@iimcb.gov.pl.

This article contains supporting information online at https://www.pnas.org/lookup/suppl/doi:10.1073/pnas.1910834117/-/DCSupplemental.

First published January 13, 2020.

and anxiety-like behavior. The latter phenotype was also reversed by inhibition of Rac1, which is potentially one of the downstream targets of TrkB.

Results

Lack of Tsc2 Leads to White Matter Disruption and Brain Dysconnectivity in Zebrafish. A disruption of WM organization is a common feature of TSC and was previously found in the telencephalon in *tsc2*$^{vu242/vu242}$ mutants (19). Indeed, when we examined the telencephalon in *tsc2*^{vu242} fish, we confirmed the presence of ectopic cell bodies in *tsc2*$^{vu242/vu242}$ by two-dimensional (2D) brain section imaging (Fig. 1*A*) and three-dimensional (3D) whole-brain imaging (*SI Appendix*, Fig. S1*A*). These cells presented higher levels of phosphorylated ribosomal protein s6 at serines 235 and 236 (P-Rps6; Fig. 1 *B* and *C* and *SI Appendix*, Fig. S1 *B*–*E*), representing the hyperactivation of mTorC1. The P-Rps6–positive cells in the pallium of *tsc2*$^{vu242/vu242}$ mutants had higher intensity signals and larger cell bodies compared with pallial cells of *tsc2*$^{+/+}$ fish (Fig. 1 *D* and *E* and *SI Appendix*, Fig. S1 *D* and *E*). We also measured the thickness of the main brain commissures because human TSC patients exhibit WM dysconnectivity that is associated with epileptic seizures and worse cognitive outcomes (12, 20–22). The *tsc2*$^{vu242/vu242}$ anterior commissure (AC) that connects the brain hemispheres in the telencephalon was thinner than in *tsc2*$^{+/+}$ fish (Fig. 2*A* and *SI Appendix*, Fig. S2*A*). The postoptic commissure was also thinner in *tsc2*$^{vu242/vu242}$ mutants, whereas the size of the lateral tracts was similar to *tsc2*$^{+/+}$ fish (*SI Appendix*, Fig. S2 *B* and *C*). The higher number of P-Rps6–positive cells negatively correlated with AC thickness, revealed by double immunostaining (Fig. 2 *A* and *B*).

To evaluate axon development that may underlie WM thinning, we crossed the *tsc2*^{vu242} line into transgenic *Tg(ptf1a:GFP)* background and examined them by live light-sheet imaging. *ptf1a:GFP*-positive neurons in the posterior tuberculum extend their axons toward the posterior commissure, where they cross the brain midline and innervate the other hemisphere (Fig. 2*C*). In *tsc2*$^{+/+}$, *ptf1a:GFP*-positive axons from one hemisphere crossed the brain boundary in one bundle. The same axons in *tsc2*$^{vu242/vu242}$ presented disturbances in tract fasciculation (Fig. 2*D*). We were able to distinguish mild axonal phenotypes (e.g., one axon did not cross the midline in the bundle) and severe disturbances in axon bundling (e.g., axons crossed the midline stochastically; *SI Appendix*, Fig. S3*A*). Quantitative morphological analysis of *ptf1a:GFP*-positive axons of *tsc2*^{vu242} confirmed the impaired tract fasciculation in *tsc2*$^{vu242/vu242}$ fish, reflected by a higher number of intersections at the midline compared with *tsc2*$^{+/+}$ (Fig. 2*E*). Moreover, *ptf1a:GFP*-positive bundles in *tsc2*$^{vu242/vu242}$ did not

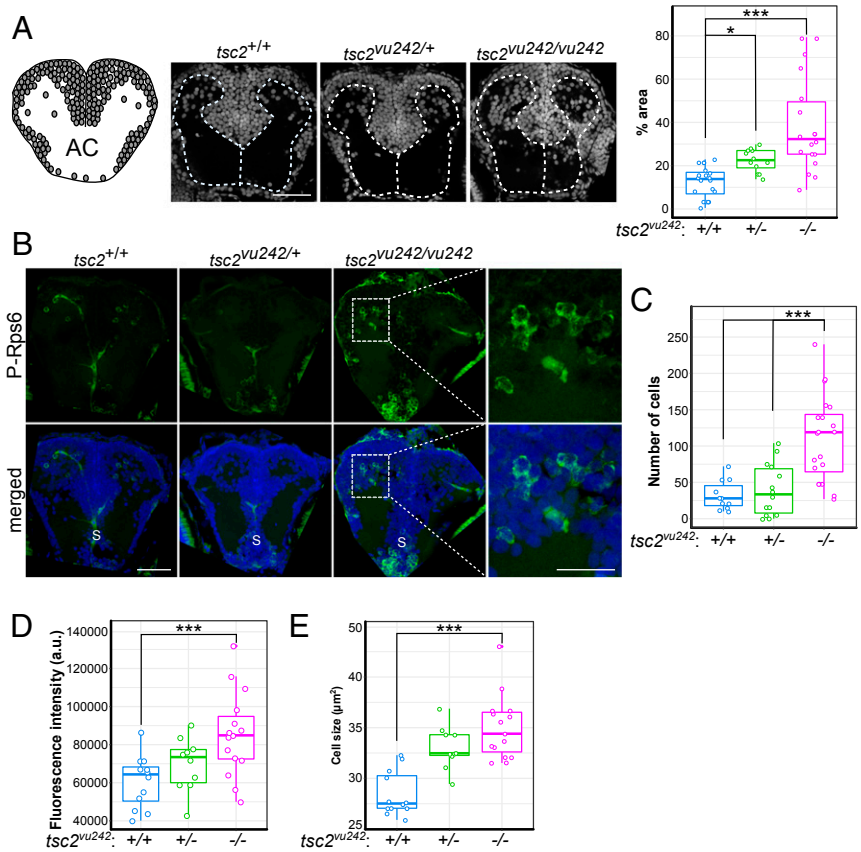

Fig. 1. *tsc2*^{vu242vul242} exhibit WM disruption and mTorC1 activation in the pallium. (*A*) Organization of gray matter and WM in coronal section through the AC. Circles represent cell bodies. Sample photographs of *tsc2*^{vu242} brain sections that were stained with DAPI are shown, together with the relative number of cell bodies in WM compartments in *tsc2*^{vu242} brains [$H = 24.443$, $P = 4.92 \times 10^{-6}$; $P = 3.1 \times 10^{-6}$ for *tsc2*$^{vu242/vu242}$ vs. *tsc2*$^{+/+}$, $P = 0.017$ for *tsc2*$^{vu242/+}$ vs. *tsc*$^{2+/+}$ (Dunn's test)]. (Scale bar, 40 μm.) (*B*) Representative images of coronal *tsc2*^{vu242} sections through the pallium that were immunostained with anti–P-Rps6 antibody (green). S, subpallium. [Scale bars, 40 and 20 μm (magnification).] (*C*) The number of P-Rps6–positive neurons in the telencephalon in *tsc2*^{vu242} [$H = 18.88$, $P = 7.95 \times 10^{-5}$; $P = 0.00071$ for *tsc2*$^{vu242/vu242}$ vs. *tsc2*$^{+/+}$, $P = 0.00117$ for *tsc2*$^{vu242/vu242}$ vs. *tsc2*$^{vu242/+}$ (Dunn's test)]. (*D*) Mean phosphorylation levels of P-Rps6 per cell per fish in the telencephalon in *tsc2*^{vu242} [$F = 6.772$, $P = 0.00335$; $P = 0.0019$ for *tsc2*$^{vu242/vu242}$ vs. *tsc2*$^{+/+}$, $P = 0.0696$ for *tsc2*$^{vu242/vu242}$ vs. *tsc2*$^{vu242/+}$ (Dunnett's test)]. (*E*) Mean soma size of P-Rps6–positive neurons per fish in the telencephalon in *tsc2*^{vu242} [$F = 21.48$, $P = 9.3 \times 10^{-7}$; $P = 4.1 \times 10^{-7}$ for *tsc2*$^{vu242/vu242}$ vs. *tsc2*$^{+/+}$, $P = 0.133$ for *tsc2*$^{vu242/vu242}$ vs. *tsc2*$^{vu242/+}$ (Dunnett's test)]. *$P < 0.05$, ***$P < 0.005$.

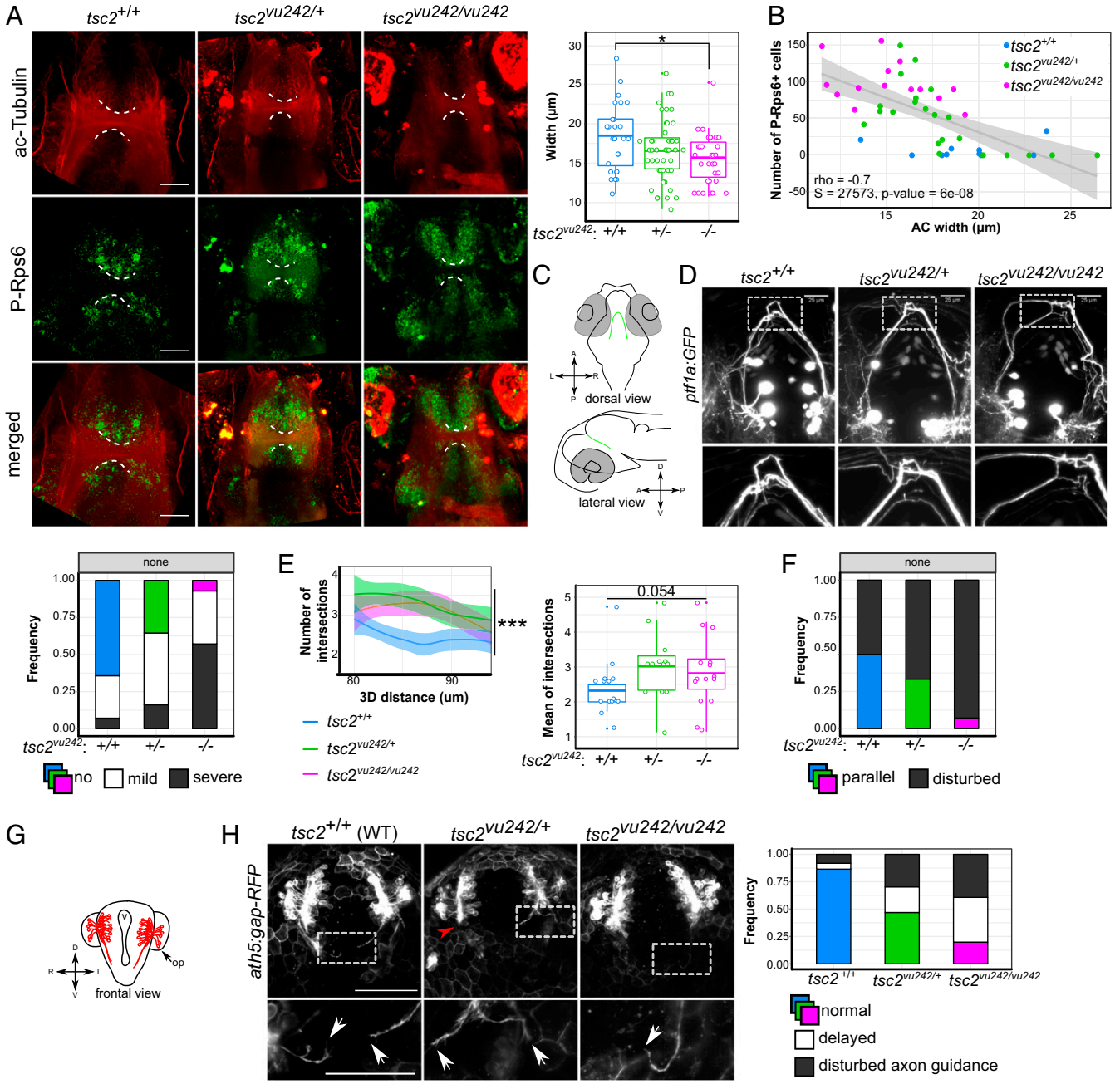

Fig. 2. $tsc2^{vu242/vu242}$ exhibit WM dysconnectivity resulting from aberrant axon elongation. (*A*) Representative horizontal optical sections through $tsc2^{vu242}$ brains that were double-immunostained with anti–acetylated-Tubulin (ac-Tubulin; red) and anti–P-Rps6 (green) antibodies that show the AC (dashed lines) at 7.5 days post fertilization, together with the quantification of the width of the AC [$F = 4.053$, $P = 0.0202$; $P = 0.011$ for $tsc2^{vu242/vu242}$ vs. $tsc2^{+/+}$ (Dunnett's test)]. (Scale bars, 30 µm.) (*B*) Correlation analysis of the number of P-Rps6–positive cells in the brain and the width of the AC, showing negative Spearman correlation and genotype clustering. (*C*) Schematic diagram of the localization of *ptf1a:GFP*-positive neurons in the posterior tuberculum that extend their axons dorsally and cross the brain midline through the posterior commissure. (*D*) Representative confocal images of a dorsal view of *ptf1a:GFP*-positive axons that show axonal tract fasciculation at the midline. The frequency of various *ptf1a:GFP* axonal phenotypes with various severity was quantified. (Scale bar, 25 µm.) (*E*) Sholl analysis of *ptf1a:GFP*-positive axon bundles at the midline of the $tsc2^{vu242}$ brains, including the number of intersections over the 3D distance from the soma [regression curves with confidence intervals; $F = 23.84$, $P = 7.4 \times 10^{-11}$; $P = 2.3 \times 10^{-6}$, $tsc2^{vu242/vu242}$ vs. $tsc2^{+/+}$ (Dunnett's test); $n = 16$ $tsc2^{vu242/vu242}$, $n = 13$ $tsc2^{vu242/+}$, $n = 15$ $tsc2^{+/+}$] and the mean number of intersections with the data distribution. For $tsc2^{+/+}$, the Sholl function converged on the value of 2 at a distance of 80 to 90 µm, representing two tracts that crossed the midline, one for each hemisphere. $tsc2^{vu242/vu242}$ fish did not present this tendency, and the average number of axons at the midline was higher than in $tsc2^{+/+}$. (*F*) Frequency of parallelization of *ptf1a:GFP* tracts from each hemisphere in the posterior commissure in the brain in $tsc2^{vu242}$ fish ($n = 27$ $tsc2^{vu242/vu242}$, $n = 31$ $tsc2^{vu242/+}$, $n = 18$ $tsc2^{+/+}$). (*G*) Schematic diagram of the localization of *ath5:gap-RFP*-positive commissures in the brain in $tsc2^{vu242}$ fish at 24 hpf. op, olfactory placodes; v, brain ventricle. (*H*) Representative confocal images of a frontal view of *ath5:gap-RFP*–positive neurons that show axon elongation (white arrows indicate axons) and the occurrence of various axonal phenotypes during olfactory medial tract development [genotype × phenotype: $F = 8.677$, $P = 8.5 \times 10^{-4}$; $P = 0.077$, $tsc2^{vu242/vu242}$ vs. $tsc2^{+/+}$ (Dunnett's test); $n = 18$ $tsc2^{vu242/vu242}$, $n = 60$ $tsc2^{vu242/+}$, $n = 25$ $tsc2^{+/+}$]. (Scale bars, 100 µm.) $^*P < 0.05$, $^{***}P < 0.005$.

form parallel tracts, in contrast to $tsc2^{+/+}$, which presented two parallel tracts (Fig. 2*F*).

To determine whether impairments in axonal development are a general phenotype of the mutants, we explored the axonal development of *ath5:gap-RFP*–positive olfactory neurons in *Tg(ath5:gap-RFP);*$tsc2^{vu242}$ zebrafish starting from 24 h post fertilization (hpf) when these neurons extended their axons to contact each other and crossed the hemisphere boundary through the AC, pioneering medial olfactory tracts (Fig. 2*G*). In living $tsc2^{vu242/vu242}$ mutants, *ath5:gap-RFP*–positive neurons more often extended their axons improperly in various directions or did not extend them at all compared with $tsc2^{+/+}$ (Fig. 2*H* and *SI Appendix*, Fig. S3*B*). This phenomenon persisted at 27 hpf, when *ath5:gap-RFP*–positive axons contacted each other at the midline, forming one tract in $tsc2^{+/+}$ fish but not in $tsc2^{vu242/vu242}$ or $tsc2^{vu242/+}$, in which they were disturbed and exhibited deficient crossing of the midline (*SI Appendix*, Fig. S3*C*). The impairments in tract fasciculation were unrelated to disturbances in glial bridges, which were properly formed at the brain midline allowing axons to cross it (*SI Appendix*, Fig. S3*D*). These findings suggest deficiencies in sensing or responding to axon guidance cues. Higher messenger RNA (mRNA) levels of the *dock3*, *dock4*, and *elmo2* genes, which are implicated in the Rac1-associated response to guidance cues, further support this hypothesis (*SI Appendix*, Fig. S4*A*). The increased expression of Dock4 and Elmo2 proteins was confirmed in the telencephalon of $tsc2^{vu242/vu242}$ compared to controls (*SI Appendix*, Fig. S4 *B–D*). In $tsc2^{vu242/vu242}$, Elmo2-positive foci were found in the AC, while they were absent there in the $tsc2^{+/+}$. Altogether, our results suggest that the lack of Tsc2 leads to commissural thinning and brain dysconnectivity, likely caused by disturbances in axon guidance signaling.

Increase in Epileptogenesis in $tsc2^{vu242/vu242}$ Zebrafish Leads to Absence Seizures. Alterations of brain connectivity may result in epileptogenesis. Thus, we examined the basal activity in $tsc2^{vu242}$ fish and confirmed decreased locomotion in $tsc2^{vu242/vu242}$ (Fig. 3*A*), which was independent of motor and vision defects (*SI Appendix*, Fig. S5 *A* and *B*). We also examined fish velocity within various ranges to describe the behavior in more detail (23). The average velocity of hyperactive movements (>2 cm/s) in $tsc2^{vu242/vu242}$ was higher than the average velocities of $tsc2^{+/+}$ or $tsc2^{vu242/+}$ fish (Fig. 3*B*), although the duration of $tsc2^{vu242/vu242}$ activity decreased within this velocity range as well (*SI Appendix*, Fig. S5*C*). These data suggest that $tsc2^{vu242/vu242}$ move in a burst-like manner, which may represent seizure-like or anxiety-like behavior.

Neuronal hyperexcitability was previously reported in the optic tectum in $tsc2^{vu242/vu242}$ fish (18). We instead examined pallium activity because the cortex in human TSC patients is thought to be the prime pathology region. We performed 3D time-lapse imaging of neuronal activity, using $tsc2^{vu242}$*;Tg(GCaMP5G)* fish. Pallial neurons in $tsc2^{vu242/vu242}$ exhibited hyperexcitability compared with controls (Fig. 3*C* and *SI Appendix*, Fig. S6*A*). We also examined fish for signs of epileptogenesis at early development as cortical malformations in TSC that lead to epileptogenesis are thought to start early. We quantified spontaneous tail flicks and body coils (STFBC) because they were previously shown to correlate with epilepsy (24). The $tsc2^{vu242/vu242}$ exhibited an increase in STFBC number (Fig. 3*D*). To further test whether $tsc2^{vu242/vu242}$ are more susceptible to seizures, we exposed $tsc2^{vu242}$ fish to γ-aminobutyric-acid receptor antagonist pentylenetetrazole (PTZ), which evokes clonic-like seizures in fish (25). $tsc2^{vu242/vu242}$ exhibited more PTZ-induced high-velocity outbursts that began much earlier than in the controls (Fig. 3 *E* and *F*).

$tsc2^{vu242/vu242}$ exhibited epileptogenesis and decreased activity, suggesting that nonmotor seizures may produce this phenotype. To test this possibility, we treated the fish with ethosuximide, a highly selective drug that is used to treat absence seizures in humans (26). Acute treatment with ethosuximide caused hyperactivity, whereas longer treatment rescued $tsc2^{vu242/vu242}$ activity to levels that were similar to controls (Fig. 3*G*). Ethosuximide also rescued early mortality of $tsc2^{vu242/vu242}$ (Fig. 3*I* and *SI Appendix*, Fig. S6*B*). However, the increase in high-speed velocity of $tsc2^{vu242/vu242}$ fish did not recover after ethosuximide (Fig. 3*H*), suggesting that complex partial seizures or anxiety are responsible for this phenotype.

$tsc2^{vu242/vu242}$ Fish Exhibit an Increase in Anxiety-Like Behavior. The increase in velocity of $tsc2^{vu242/vu242}$ may represent anxiety-like behavior, which has not been previously reported in Tsc2-deficient zebrafish. We observed disturbances in the axonal development of *ptf1a:GFP*-positive neurons in the posterior tuberculum in $tsc2^{vu242/vu242}$ (Fig. 2 *D–F*), which may result in alterations of connectivity of the fear/anxiety response axis (27). We evaluated whether $tsc2^{vu242/vu242}$ exhibit anxiety-like behavior by subjecting $tsc2^{vu242}$ fish to a light-preference test. $tsc2^{+/+}$ fish spent more time in the light compartment, reflecting phototaxia. $tsc2^{vu242/vu242}$ spent more time in the dark compartment compared with $tsc2^{+/+}$ (Fig. 4*A*), indicating that they were indifferent to light and implying decreased anxiety-like behavior. We also found that $tsc2^{vu242/vu242}$ movements were more confined to the peripheral areas of the well compared with $tsc2^{+/+}$, suggesting increased anxiety-like behavior. We then analyzed the activity of $tsc2^{vu242}$ fish in an open field to test anxiety-like behavior that is related to a novel environment and open areas. $tsc2^{vu242/vu242}$ spent less time exploring and spent more time near the edges compared with $tsc2^{+/+}$ (Fig. 4*B*), suggesting increased anxiety-like behavior.

Phototaxic zebrafish larvae exhibit anxiety-like behavior when subjected to a dark environment, resulting in hyperactivity. Switching the light on causes freezing because the sudden change in lighting conditions augments anxiety-like behavior even further, which is innately perceived by the fish as dangerous (27). $tsc2^{vu242/vu242}$ mutants exhibited increased activity in the dark environment compared with $tsc2^{+/+}$. These mutants also exhibited slightly more freezing during light, but this increase was not significantly different from $tsc2^{+/+}$, which already presented very low activity (Fig. 4*C*). To validate the experimental setup, we subjected $tsc2^{vu242}$ fish to anxiolytic diazepam or anxiogenic retinoic acid (RA). Diazepam decreased anxiety-like behavior in both the $tsc2^{vu242/vu242}$ and their control siblings, whereas RA increased anxiety-like behavior in $tsc2^{+/+}$ and $tsc2^{vu242/+}$. However, RA did not significantly affect $tsc2^{vu242/vu242}$, which had already exhibited increased anxiety-like behavior (Fig. 4*D* and *SI Appendix*, Fig. S7). These results were corroborated by changes in the amplitude of activity between light phases (Fig. 4*E*). Finally, cortisol levels in $tsc2^{vu242/vu242}$ fish were elevated compared with their control siblings (Fig. 4*F*).

The results from the light-preference test (Fig. 4*A*), sudden-light-changes test (Fig. 4*C*), and cortisol levels (Fig. 4*F*) suggest impairment in impulse control that contrasts with the anxiety hypothesis. To resolve this, we evaluated escape responses to repeated dark flashes and their habituation. The $tsc2^{vu242/vu242}$ exhibited lower or delayed responses to the first startle stimulus compared with $tsc2^{+/+}$, but the startle habituation was similar to that of other fish (*SI Appendix*, Fig. S8). Although the total activity of $tsc2^{vu242/vu242}$ was lower, the fish indeed exhibited a startle response but to a lesser extent than sibling controls. These results do not confirm higher impulsivity and instead suggest that freezing behavior in response to the startle stimulus was attributable to higher preexisting levels of anxiety in $tsc2^{vu242/vu242}$. Altogether, the results confirm increased anxiety-like behavior in $tsc2^{vu242/vu242}$ compared with $tsc2^{+/+}$ and recapitulate the human phenotype of TANDs (4).

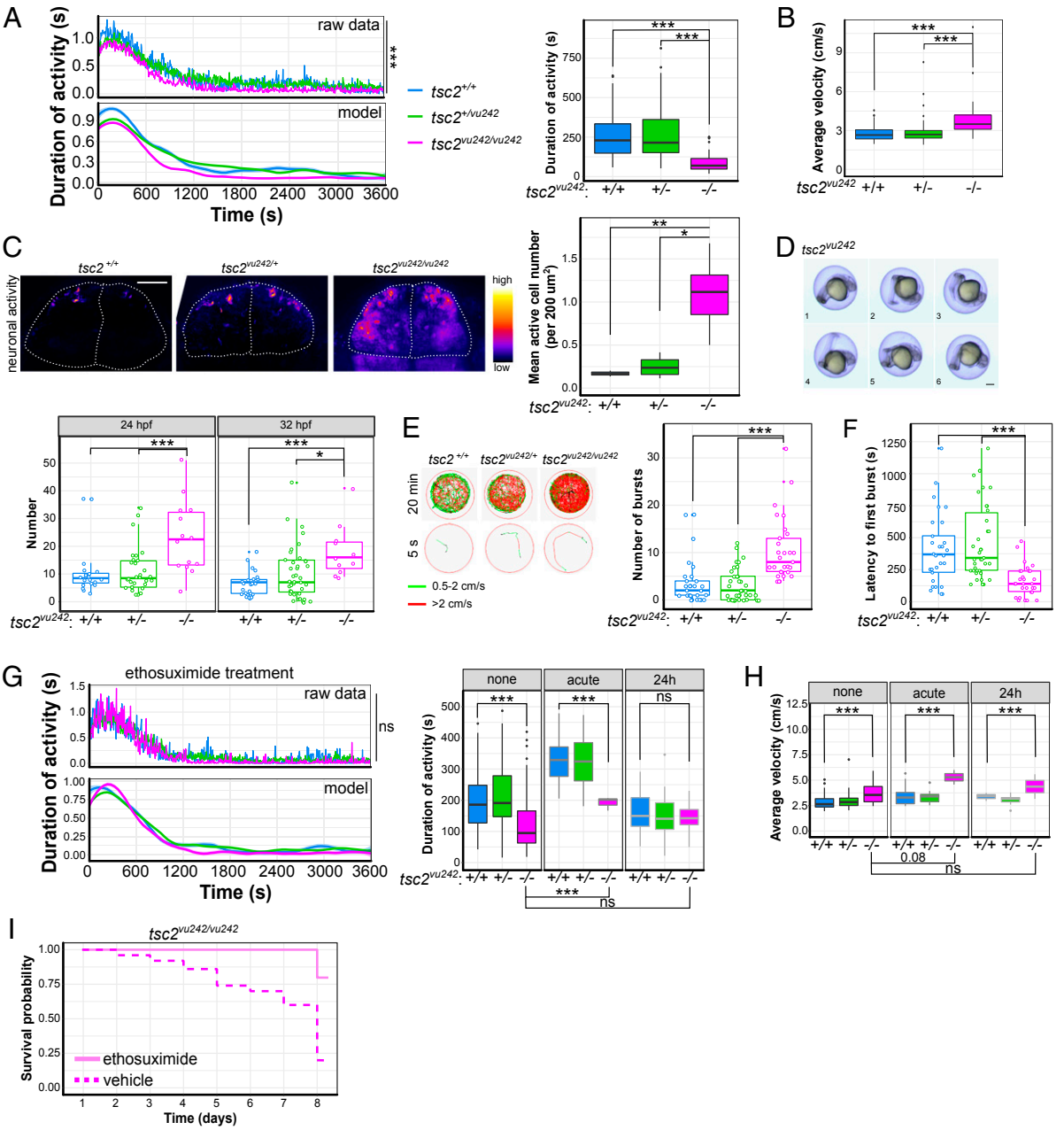

Fig. 3. *tsc2*$^{vu242/vu242}$ exhibit decrease in activity, increase in epileptogenesis, and increase in response to ethosuximide treatment. (*A*) Activity analysis of *tsc2*^{vu242} fish that shows activity vs. time [$F = 2.601$, $P = 0.0067$; $P = 2.38 \times 10^{-9}$ for *tsc2*$^{vu242/vu242}$ vs. *tsc2*$^{+/+}$, $P = 7.42 \times 10^{-6}$ for *tsc2*$^{vu242/vu242}$ vs. *tsc2*$^{vu242/+}$ (Dunnett's test)] and cumulative activity [$F = 18.61$, $P = 4.76 \times 10^{-8}$; $P = 4.16 \times 10^{-8}$ for *tsc2*$^{vu242/vu242}$ vs. *tsc2*$^{vu242/+}$, $P = 1.22 \times 10^{-6}$ for *tsc2*$^{vu242/vu242}$ vs. *tsc2*$^{+/+}$ (Dunnett's test)] in *tsc2*$^{vu242/vu242}$ fish ($n = 32$) compared with *tsc2*$^{vu242/+}$ fish ($n = 85$) and *tsc2*$^{+/+}$ control siblings ($n = 50$) during 1 h of tracking. (*B*) Average velocity of high-velocity movements (>2 cm/s) of *tsc2*$^{vu242/vu242}$ fish compared with *tsc2*$^{vu242/+}$ and *tsc2*$^{+/+}$ controls [$H = 31.73$, $P = 1.29 \times 10^{-7}$; $P = 4.8 \times 10^{-6}$ for *tsc2*$^{vu242/vu242}$ vs. *tsc2*$^{+/+}$, $P = 2.1 \times 10^{-7}$ for *tsc2*$^{vu242/vu242}$ vs. *tsc2*$^{vu242/+}$ (Dunn's test)]. (*C*) Representative images that show neuronal activity (without any stimulation) in the pallium in *tsc2*^{vu242} fish and the mean number of active cells, which increases in *tsc2*$^{vu242/vu242}$ [$F = 9.638$, $P = 0.0074$; $P = 0.009$ for *tsc2*$^{vu242/vu242}$ vs. *tsc2*$^{+/+}$, $P = 0.012$ for *tsc2*$^{vu242/vu242}$ vs. *tsc2*$^{+/vu242}$ (Dunnett's test)]. (Scale bar, 30 μm.) (*D*) Exemplary time-lapse photographs of STFBC of *tsc2*^{vu242} fish and quantification at 24 hpf [$F = 8.59$, $P = 5 \times 10^{-4}$; $P \leq 0.001$ for *tsc2*$^{vu242/vu242}$ vs. other genotypes (Dunnett's test)] and 32 hpf [$F = 7.535$, $P = 0.001$; $P = 0.012$ for *tsc2*$^{vu242/vu242}$ vs. *tsc2*$^{vu242/+}$, $P = 4 \times 10^{-4}$ for *tsc2*$^{vu242/vu242}$ vs. *tsc2*$^{+/+}$ (Dunnett's test)]. (Scale bar, 100 μm.) (*E*) Representative tracks for each *tsc2*^{vu242} genotype after treatment with PTZ representing the entire 20 min and the first 5 s of tracking, showing the number of PTZ-induced seizure-like outbursts in the first 10 min of tracking for *tsc2*$^{vu242/vu242}$ fish compared with *tsc2*$^{vu242/+}$ and *tsc2*$^{+/+}$ fish [$H = 34.667$, $P = 3 \times 10^{-8}$; $P = 6.8 \times 10^{-6}$ for *tsc2*$^{vu242/vu242}$ vs. *tsc2*$^{+/+}$, $P = 9.1 \times 10^{-8}$ for *tsc2*$^{vu242/vu242}$ vs. *tsc2*$^{vu242/+}$ (Dunn's test)]. Red tracks represent high-velocity movements (>2 cm/s). Green tracks indicate free swimming (movement within a range of 0.5 to 2 cm/s). Black tracks indicate free floating (<0.5 cm/s). (*F*) Time to first PTZ-induced outburst for *tsc2*$^{vu242/vu242}$ compared with control siblings [$H = 26.838$, $P = 1.49 \times 10^{-6}$; $P = 3 \times 10^{-4}$ for *tsc2*$^{vu242/vu242}$ vs. *tsc2*$^{+/+}$, $P = 2.1 \times 10^{-6}$ for *tsc2*$^{vu242/vu242}$ vs. *tsc2*$^{vu242/+}$ (Dunn's test)]. (*G*) Activity analysis of *tsc2*^{vu242} fish that were treated with ethosuximide, showing activity vs. time and cumulative activity of *tsc2*$^{vu242/vu242}$ ($n = 32$) compared with *tsc2*$^{vu242/+}$ ($n = 56$) and *tsc2*$^{+/+}$ ($n = 25$) over 1 h of tracking. An increase in activity after acute ethosuximide treatment is considered to represent anxiety-like behavior, reflected by hyperactivity regardless of genotype ($H = 40.312$, $P = 9.15 \times 10^{-9}$; $P = 3.9 \times 10^{-9}$ for *tsc2*$^{vu242/vu242}$ untreated vs. treated with ethosuximide acutely, $P > 0.05$ for *tsc2*$^{vu242/vu242}$ untreated vs. treated with ethosuximide for 24 h [Dunn's test]). (*H*) Average velocity of high-velocity movements (>2 cm/s) of *tsc2*$^{vu242/vu242}$ compared with *tsc2*$^{vu242/+}$ and *tsc2*$^{+/+}$ fish after ethosuximide treatment [$H = 9.5556$, $P = 0.02275$; $P = 0.08$ for *tsc2*$^{vu242/vu242}$ untreated vs. treated with ethosuximide acutely, $P > 0.05$ for *tsc2*$^{vu242/vu242}$ untreated vs. treated with ethosuximide for 24 h (Dunn's test)]. (*I*) Survival probability of *tsc2*$^{vu242/tsc2vu242}$ fish after ethosuximide treatment vs. vehicle treatment. *$P < 0.05$, **$P < 0.01$, ***$P < 0.005$.

TrkB Antagonist ANA-12 Reverses TSC-Associated Phenotypes in Zebrafish. Brain-derived neurotrophic factor (BDNF)-TrkB signaling has not been previously studied in the context of TSC, although the dysregulation of this pathway has been implicated in cell migration, axonal growth, epilepsy, and anxiety (26, 28, 29). Thus, we tested whether targeting TrkB reverses the TSC-related phenotypes that are observed in *tsc2*$^{vu242/vu242}$. ANA-12 is a selective antagonist of TrkB and was previously shown to exhibit anxiolytic potential in mice (29). To test the effects of ANA-12, we first examined the phosphorylation levels of TrkB by enzyme-linked immunosorbent assay (ELISA). The amino acid sequence of zebrafish TrkB shares over 60% homology with the human sequence, with highly conserved tyrosine phosphorylation motives (*SI Appendix*, Fig. S9*A*), which are phosphorylated upon TrkB activation. The phosphorylated TrkB (P-TrkB) levels were higher in *tsc2*$^{vu242/vu242}$ compared with *tsc2*$^{+/+}$ and lower after ANA-12 treatment (Fig. 5*A*). To further confirm the actions of ANA-12 on the TrkB-signaling pathway, we examined the activation of cAMP-response element-binding protein (Creb), which depends on BDNF-induced TrkB activation. Creb phosphorylation at Ser111, homologous to Ser133 in mammals, was increased in *tsc2*$^{vu242/vu242}$ compared with controls, and ANA-12 treatment reversed this (Fig. 5*B* and *SI Appendix*, Fig. S9*B*). These results suggest that ANA-12 produces similar effects in mammals and fish through TrkB and Creb.

Treatment with ANA-12 increased survival of *tsc2*$^{vu242/vu242}$ mutants more than treatment with vigabatrin (VGN), which is the first-line drug for the treatment of TSC-associated epilepsy. However, ANA-12 was not as effective in restoring survival of *tsc2*$^{vu242/vu242}$ as pretreatment with the direct mTorC1 inhibitor rapamycin (RapaP) or pretreatment with VGN (VGN-P; Fig. 5*C* and *SI Appendix*, Fig. S10 *A* and *B*). ANA-12 did not alter activation of the mTorC1 pathway in the brain of *tsc2*$^{vu242/vu242}$ (Fig. 5*D*) but restored the proper width of the AC when administered at 48 hpf, similar to the effect of RapaP (Fig. 5*E* and *SI Appendix*, Fig. S10*C*). Moreover, the seizure-associated decreased activity of *tsc2*$^{vu242/vu242}$ was rescued by ANA-12 as potently as by VGN or Rapa-P (Fig. 5 *F*–*H*). ANA-12 also decreased the number of PTZ-induced bursts and increased time without bursting (*SI Appendix*, Fig. S10*D*). The increased high-range velocity in *tsc2*$^{vu242/vu242}$, reflecting anxiety-like behavior, was fully rescued only by ANA-12 treatment as well (Fig. 5 *I*–*K*). Moreover, VGN did not alter the increase in high-range velocity in mutant fish (Fig. 5*K*), further suggesting that the increase in velocity was not caused by partial seizures but indeed reflected anxiety-like behavior. Therefore, reducing TrkB signaling effectively treated both epilepsy- and anxiety-associated behavioral changes and brain dysconnectivity.

The above-described droplet digital PCR (ddPCR) results (*SI Appendix*, Fig. S4*A*) pointed to Dock-Elmo-Rac1 pathway up-regulation. TrkB activates the Rac1 pathway in neurons (30); thus we hypothesized that up-regulation of Rac1 activity contributes to the *tsc2*$^{vu242/vu242}$ phenotype. Treatment with the Rac1 inhibitor W56 (200 nM) did not affect total activity but resulted in lower high-range velocity of *tsc2*$^{vu242/vu242}$ compared to *tsc2*$^{+/+}$ (*SI Appendix*, Fig. S10 *E* and *F*), thereby rescuing an anxiety-like parameter. Collectively, our data implicate TrkB hyperactivity in many aspects of TSC pathology, suggesting also a role for Rac1 in TSC-related anxiety.

Discussion

TSC symptoms arise during brain development through mechanisms that are not fully understood. In the present study, *tsc2*$^{vu242/vu242}$ exhibited pallium malformations and thinner commissures, which were rescued by TrkB inhibition, together with behavioral abnormalities, suggesting that the observed neurological phenotypes were related to neuroanatomical changes.

The thinner AC width in *tsc2*$^{vu242/vu242}$ mutants may reflect the WM thinning seen in TSC patients, which is associated with seizures (12, 20–22). In TSC patients, decreased density of the corpus callosum is correlated with epilepsy and such TANDs as autism and ID (22). Moreover, patients with TSC-associated refractory epilepsy have thinner and disorganized axon tracts (12). Similar fasciculation disturbances were seen in *tsc2*$^{vu242/vu242}$ *ptf1a:GFP*-positive axons in the present study. These disturbances may result from impairments in axonal pathfinding and elongation. Consistently, previous studies found that lack of Tsc1 induces ectopic axons in vitro and WM defects in mice (31). The axon guidance pathways are regulated by external cues and their receptors that in turn activate a Dock–Elmo protein complex that subsequently activates Rac1, resulting in actin dynamics. Dock-3 and Dock-4 play pivotal roles in axon development. Dock-3 promotes axonal growth, forming the conventional Dock–Elmo complex, which is important for Rac1 activation in response to BDNF–TrkB signaling. Dock-4 promotes neurite differentiation to establish axon-dendrite polarity (32). Interestingly, in the present study, *dock3*, *dock4*, *elmo2*, and *rac1* mRNA levels were higher in *tsc2*$^{vu242/vu242}$ than in *tsc2*$^{+/+}$. We further confirmed increased Dock4- and Elmo2-protein levels in *tsc2*$^{vu242/vu242}$ fish brains. Moreover, inhibition of Rac1 rescued anxiety-related *tsc2*$^{vu242/vu242}$ velocity, but did not affect decreased locomotion, suggesting that Rac1 involvement in anxiety-related behavior is separate from epilepsy.

Recently, zebrafish has become an accepted model for neuropsychiatric studies having applications in translational research. Zebrafish as highly complex vertebrates present a repertoire of complicated behaviors that can be used to study neurological and neuropsychiatric human disorders (33, 34). In the present study, *tsc2*$^{vu242/vu242}$ mutants exhibited lower activity but higher high-range velocity, suggesting that they swam in a burst-like manner. These high-amplitude movements can be caused by such TAND-related phenotypes as overactivity, impaired impulse control, or anxiety. Increased high-range velocity cannot represent hyperactivity because *tsc2*$^{vu242/vu242}$ total locomotion decreased. We hypothesized that the increased velocity of *tsc2*$^{vu242/vu242}$ resulted from anxiety-like behavior and the open field, sudden-light changes test and elevated cortisol levels confirmed this. However, the increased velocity could be potentially caused by impaired impulse control, which could explain the results of the light-preference test (higher risk taking and boldness) and would contradict the results of the open field. Impaired impulsivity would possibly result in elevated cortisol and hyperactive bursts, similar to the effects produced by anxiety. Therefore, we performed a startle analysis to repeated dark flashes which is relevant to anxiety, impulsivity, and ID reflected by escape responses to startling stimuli and habituation after repetition. *tsc2*$^{vu242/vu242}$ exhibited lower or delayed response to the first startle stimulus compared with *tsc2*$^{+/+}$ that exhibited no difference in habituation. This did not confirm higher impulsivity in *tsc2*$^{vu242/vu242}$ and further suggested anxiety as a cause for the observed phenotypes.

Because *tsc2*$^{vu242/vu242}$ fish remained at the edges of the well in the light–dark test, we propose that *tsc2*$^{vu242/vu242}$ suffer brain impairments and cannot react to dark conditions similarly to *tsc2*$^{+/+}$. Startle response results do not necessarily contradict this hypothesis. Although we did not see differences in habituation of the *tsc2*$^{vu242/vu242}$ response compared with controls, the response to the startling stimulus was already impaired. Supporting the possibility of ID, we found perturbances in the fasciculation of *ptf1a:GFP*-positive tracts from the posterior tuberculum in *tsc2*$^{vu242/vu242}$, which may impair anxiety regulation. Another brain part, the habenula, is critical for processing emotions, social behavior, anxiety responses, and locomotion, and it is thought to act as a link between the forebrain and midbrain to produce emotional responses (35–37). The left habenula has

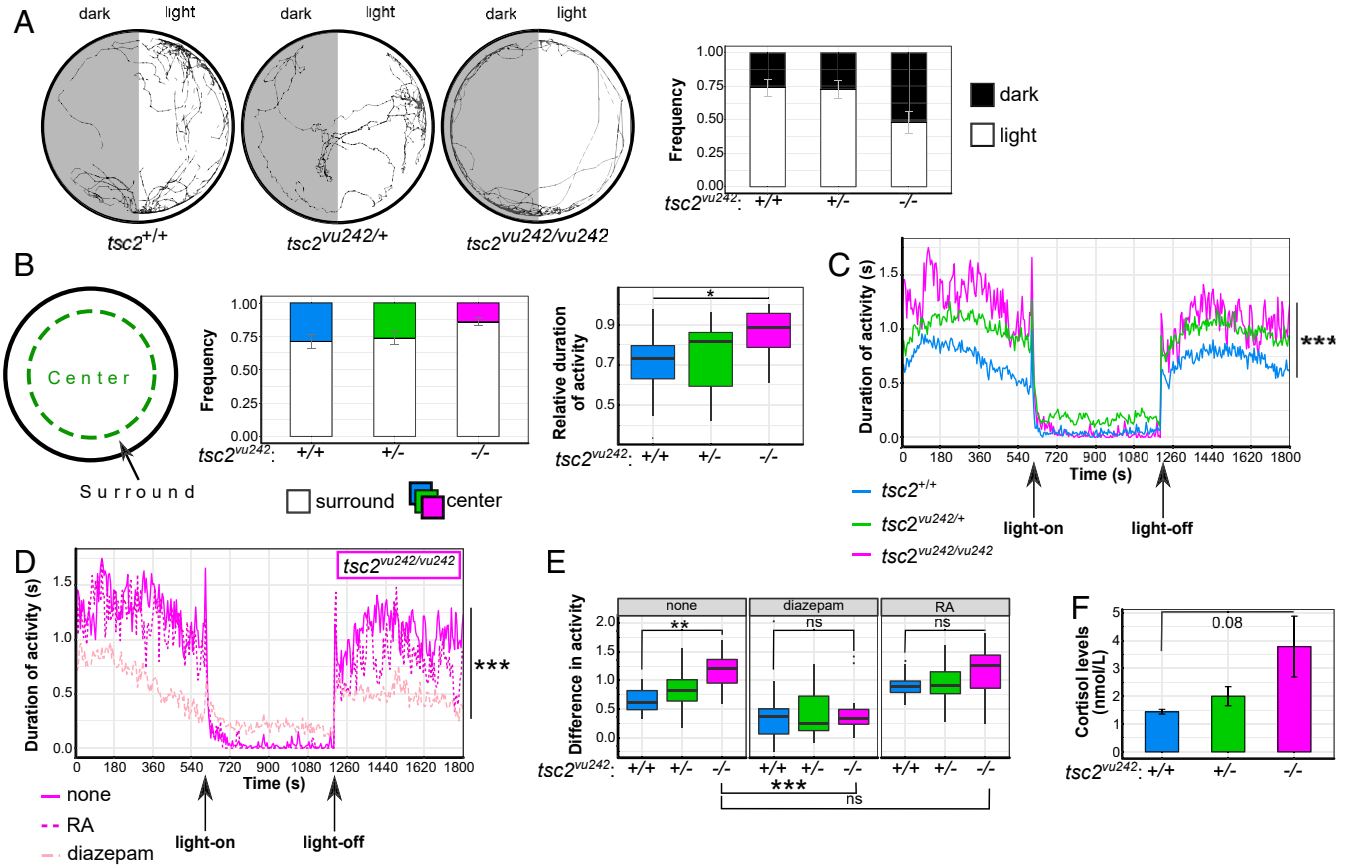

Fig. 4. Mutant $tsc2^{vu242/vu242}$ exhibit an increase in anxiety-like behavior in the open field and in response to sudden changes in light conditions and an increase in cortisol levels. (*A*) Light-preference analysis of $tsc2^{vu242}$ fish, including representative tracks and time spent in the light and dark compartments (relative to total activity) for each $tsc2^{vu242}$ genotype [genotype × treatment: $F = 8.181$, $P = 5 \times 10^{-4}$; $P = 1 \times 10^{-4}$ for $tsc2^{+/+}$ light vs. dark, $P = 3 \times 10^{-4}$ for $tsc2^{vu242/+}$ light vs. dark, $P = 0.999$ for $tsc2^{vu242/vu242}$ light vs. dark (Tukey HSD test); $n = 15$/genotype]. The data are expressed as mean ± SEM. (*B*) Schematic diagram of the open field analysis of $tsc2^{vu242}$ fish that shows selections of the peripheral (surround) and central (center) areas of the experimental well, time spent in the peripheral and central areas of the well (relative to total activity) for each $tsc2^{vu242}$ genotype (mean ± SEM), and data distribution of the time spent in the peripheral area relative to total activity of $tsc2^{vu242}$ fish [$F = 3.721$, $P = 0.0321$; $P = 0.043$ for $tsc2^{vu242/vu242}$ vs. $tsc2^{+/+}$, $P = 0.11$ for $tsc2^{vu242/vu242}$ vs. $tsc2^{vu242/+}$ (Tukey HSD test); $n = 15$/genotype]. (*C*) Mean activity over time for each $tsc2^{vu242}$ genotype after sudden changes in light conditions [$H = 636.14$, $P < 2.2 \times 10^{-16}$; $P < 7.4 \times 10^{-8}$ for $tsc2^{vu242/vu242}$ vs. $tsc2^{+/+}$ or $tsc2^{vu242/+}$ (Dunn's test); $n = 23$ $tsc2^{vu242/vu242}$, $n = 69$ $tsc2^{vu242/+}$, $n = 45$ $tsc2^{+/+}$]. (*D*) Mean activity over time for $tsc2^{vu242/vu242}$ that were subjected to sudden changes in light conditions after treatment with anxiety-modulating drugs compared with untreated fish [$H = 492.92$, $P < 2.2 \times 10^{-16}$; $P < 2 \times 10^{-16}$, untreated vs. treated (Dunn's test)]. (*E*) Amplitudes of activity in the dark and light phases in $tsc2^{vu242}$ fish after treatment with various anxiety-modulating drugs compared with untreated fish [genotype × treatment: $F = 1.806$, $P = 0.128$; treatment: $F = 43.643$, $P < 2 \times 10^{-16}$; $P = 0.0067$ for untreated $tsc2^{vu242/vu242}$ vs. $tsc2^{+/+}$; $P = 1.3 \times 10^{-5}$ for untreated $tsc2^{vu242/vu242}$ vs. treated with diazepam; $P = 0.999$, untreated $tsc2^{vu242/vu242}$ vs. treated with RA (Tukey HSD test)]. (*F*) Quantification of cortisol levels in $tsc2^{vu242}$ fish [$F = 3.395$, $P = 0.103$; $P = 0.081$, $tsc2^{vu242/vu242}$ vs. $tsc2^{+/+}$ (Dunnett's test); $n = 120$/genotype]. *$P < 0.05$, **$P < 0.01$, ***$P < 0.005$, ns: not significant.

been shown to regulate light preference behavior in zebrafish larvae (38). Other left–right asymmetries in brain morphology have also been linked to regulation of boldness and exploratory behavior (39). Therefore, it is likely that aberrant development of the brain hemisphere connections is responsible for the observed TAND-related phenotypes. Both the increased anxiety-like behavior in the open field and when subjected to sudden changes in light and the lack of light preference in $tsc2^{vu242/vu242}$ may thus result from disturbances in overall connectivity to the habenula.

Anxiety-like behavior can be induced by seizures (40), providing a link between epileptogenesis, seizures, and anxiety. Reductions of BDNF signaling in the hippocampus were shown to prevent spontaneous seizures and rescue anxiety-like behavior in rodent epilepsy models (26). Consistently, sustained Creb activity was shown to produce seizures in mice (41). In the present study, ANA-12 treatment rescued the activity impairment and reversed increased high-range velocity in $tsc2^{vu242/vu242}$. At the same time, ANA-12 also reduced TrkB and Creb activation and lowered the seizure threshold in $tsc2^{vu242/vu242}$, implicating TrkB signaling in epileptogenesis.

Reversal of AC thinning and anxiety-related hypervelocity by ANA-12 but not by VGN suggests that commissural connections substantially contribute to regulating anxiety and links brain anatomy with behavior. These results also implicate TrkB hyperactivity in both commissure development and anxiety. We also showed that Rac1 inhibition, similar to inhibition of TrkB, rescued anxiety-related velocity of $tsc2^{vu242/vu242}$. In line with our results, Rac1 overactivation was previously shown to inhibit the formation of long-term fear conditioning memory (42). Rac1 is required for commissural axon development specifically in the cortex and controls axon crossing through the AC and corpus callosum in mice (43, 44). $tsc2^{vu242/vu242}$ exhibited thinner AC and presented problems with axons crossing the brain midline. Therefore, it is probable that the disruption of commissural axons results in anxiety through Rac1. Moreover, Rac1 may act downstream of TrkB in axon development and synaptic crosstalk (30, 45, 46), raising an intriguing possibility that, also in TSC,

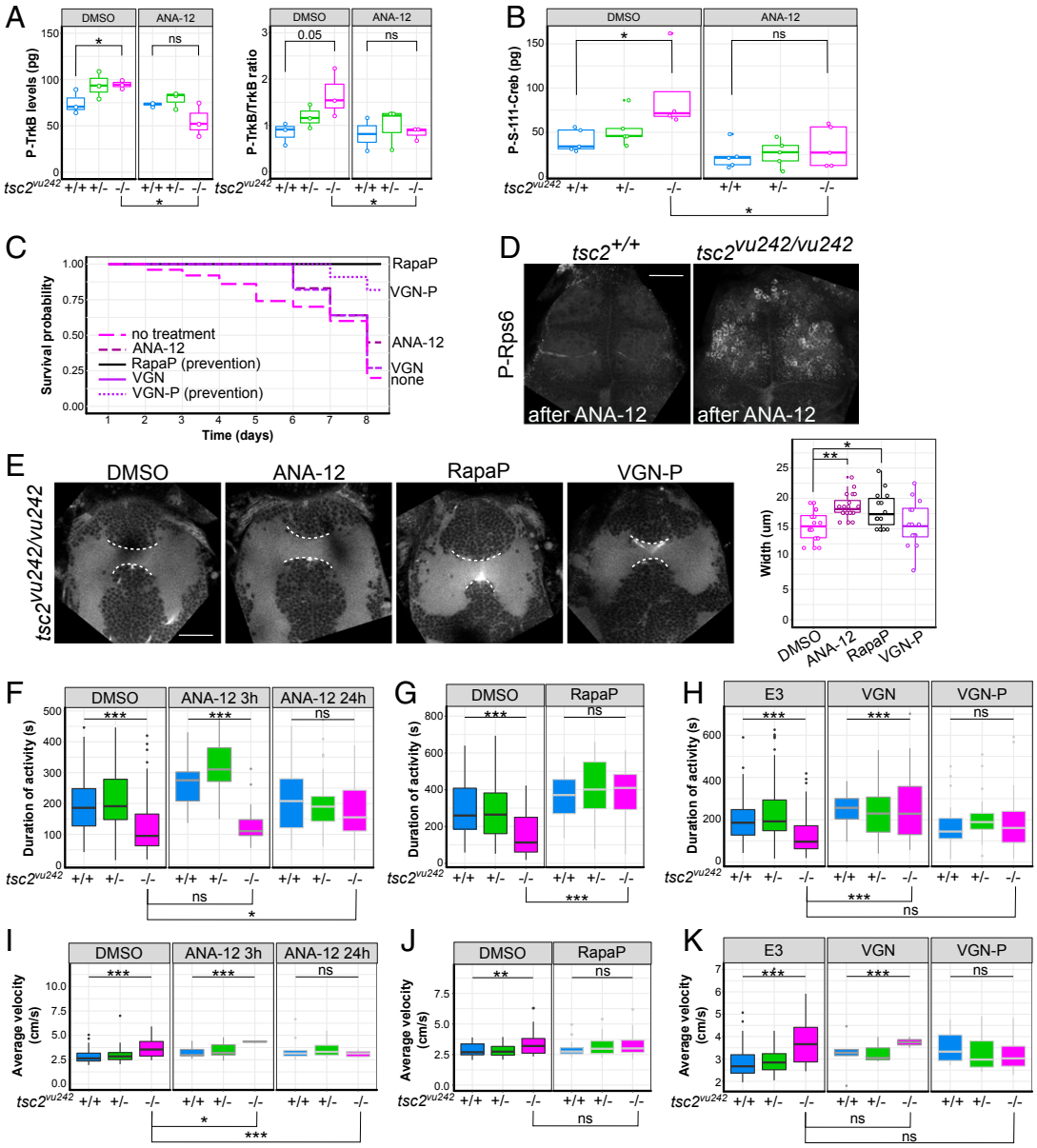

Fig. 5. ANA-12 rescues survival, brain dysconnectivity, impairment in locomotion, and anxiety-related hypervelocity in $tsc2^{vu242vul242}$ mutants. (*A*) Quantification of activation of TrkB receptor judged by levels of P-TrkB and ratio of P-TrkB to TrkB by immunochemistry (ELISA) revealed higher activation levels in $tsc2^{vu242/vu242}$ fish compared with control siblings and a decrease after ANA-12 treatment [P-TrkB: $H = 4.355$, $P = 0.049$; $P = 0.05$, $tsc2^{vu242/vu242}$ vs. $tsc2^{+/+}$ (Dunn's test)]; $P = 0.015$, $tsc2^{vu242/vu242}$ untreated vs. treated with ANA-12 (Dunn's test); P-TrkB/TrkB: $H = 5.689$, $P = 0.05$; $P = 0.05$, $tsc2^{vu242/vu242}$ vs. $tsc2^{+/+}$ (Dunn's test); $P = 0.049$, $tsc2^{vu242/vu242}$ untreated vs. treated with ANA-12 (Dunn's test)]. (*B*) Quantification of levels of Creb phosphorylation by immunochemistry (ELISA) revealed higher levels in $tsc2^{vu242/vu242}$ compared with controls and a decrease after ANA-12 treatment [genotype: $F = 3.513$, $P = 4.66 \times 10^{-4}$; treatment: $F = 14.759$, $P = 8.33 \times 10^{-4}$; genotype × treatment: $P > 0.05$; $P = 0.012$, $tsc2^{vu242/vu242}$ after ANA-12 vs. DMSO treatment (Tukey HSD test); $P = 0.033$, untreated $tsc2^{vu242/vu242}$ vs. $tsc2^{+/+}$ (Tukey HSD test)]. (*C*) Survival probability of $tsc2^{vu242/vu242}$ after various treatments. (*D*) Confocal images of $tsc2^{vu242}$ brains that were immunostained with anti–P-Rps6 antibody after ANA-12 treatment. (Scale bar, 30 μm.) (*E*) AC width in $tsc2^{vu242/vu242}$ after various treatments, including representative confocal images and quantification [$F = 5.83$, $P = 0.00142$; $P = 0.002$ for DMSO vs. ANA-12, $P = 0.049$ for DMSO vs. Rapa pretreatment (Dunnett's test)]. (Scale bar, 30 μm.) (*F*) Cumulative activity of $tsc2^{vu242/vu242}$ after treatment with ANA-12 compared with $tsc2^{vu242/+}$ and $tsc2^{+/+}$ fish over 1 h of tracking, showing an increase in activity of mutant fish after treatment [$H = 16.652$, $P = 2.42 \times 10^{-4}$; $P = 0.0172$, $tsc2^{vu242/vu242}$ untreated vs. treated with ANA-12 for 24 h (Dunn's test)]. (*G*) Cumulative activity of the $tsc2^{vu242/vu242}$ after the prevention of disease development by Rapa pretreatment compared with $tsc2^{vu242/+}$ and $tsc2^{+/+}$ fish over 1 h of tracking, showing an increase in activity of mutant fish after treatment [$H = 32.18$, $P = 3.9 \times 10^{-8}$; $P = 2.0 \times 10^{-8}$ for $tsc2^{vu242/vu242}$ untreated vs. rapamycin pretreatment (Dunn's test)]. (*H*) Cumulative activity of $tsc2^{vu242/vu242}$ after the treatment with VGN or VGN-P to prevent disease development, respectively, compared with $tsc2^{vu242/+}$ and $tsc2^{+/+}$ fish over 1 h of tracking, showing improvements in activity after short VGN treatment but toxicity after longer treatment with VGN [$H = 19.262$, $P = 6.566 \times 10^{-5}$; $P = 3.4 \times 10^{-5}$ for $tsc2^{vu242/vu242}$ untreated vs. treated with VGN, $P > 0.05$ for $tsc2^{vu242/vu242}$ untreated vs. VGN-P (Dunn's test)]. (*I*) Average velocity of high-velocity movements of $tsc2^{vu242/vu242}$ compared with $tsc2^{vu242/+}$ and $tsc2^{+/+}$ fish after treatment with ANA-12 [$H = 14.686$, $P = 6.47 \times 10^{-4}$; $P = 0.015$ for $tsc2^{vu242/vu242}$ untreated vs. treated with ANA-12 for 3 h, $P = 0.003$ for $tsc2^{vu242/vu242}$ untreated vs. treated with ANA-12 for 24 h (Dunn's test)]. (*J*) Average velocity of high-velocity movements of $tsc2^{vu242/vu242}$ fish after the prevention of disease development with Rapa pretreatment compared with $tsc2^{vu242/+}$ and $tsc2^{+/+}$ fish [$H = 29.68$, $P = 4.52 \times 10^{-5}$; $P > 0.05$ for $tsc2^{vu242/vu242}$ untreated vs. $tsc2^{vu242/vu242}$ with Rapa pretreatment (Dunn's test)]. (*K*) Average velocity of high-velocity movements of $tsc2^{vu242/vu242}$ after the treatment with VGN or VGN-P to prevent disease development, respectively, compared with $tsc2^{vu242/+}$ and $tsc2^{+/+}$ fish ($H = 3.286$, $P = 0.19$). *$P < 0.05$, **$P < 0.01$, ***$P < 0.005$, ns: not significant.

TrkB hyperactivity results in anxiety, causing Rac1 pathway dysregulation. Nevertheless, hyperactive Rac1/3 also caused excitatory–inhibitory imbalance and increased brain activity with impaired synchronization (47). This is coherent with our results as *tsc2*$^{vu242/vu242}$ exhibited higher brain activity and seizures. However, it is also possible that Rac1 affects anxiety by impairing synaptic crosstalk in other brain regions, independently from commissures. Finally, although we do see similar effects of ANA-12 and Rac1 inhibitors on anxiety-like behavior in zebrafish and it is plausible that their targets act in one pathway, we only hypothesize a direct link. In conclusion, the presented results implicate TrkB and Rac1 signaling in the pathology of TSC, expanding our understanding of the complex mechanisms that underlie this disease and revealing a potential therapeutic target.

Methods

Drug Treatments. PTZ, RA, VGN, ethosuximide, and ANA-12 were purchased from Sigma-Aldrich. Rapamycin, diazepam, and W56 were obtained from MBL International, Cefarm S.A, and Tocris, respectively. Drugs were dissolved in E3, dimethylsulfoxide (DMSO), or glycerol for stock solutions, and were further diluted in E3. Drugs were administered directly into E3 with the same number of dechorionated fish. More information can be found in *SI Appendix*.

Image Acquisition and Analyses. Fluorescence images of cryosections and whole mounts were acquired with a Zeiss LSM800 confocal microscope. For STFBC, living embryos in the chorions were recorded using a Leica M60 microscope with a DMC2900 camera every 10 ms for 3 min. Other in vivo imaging was performed with a Lighsheet Z.1 microscope (Zeiss). Image analyses were performed using Fiji (fiji.sc) (48) with a measurement tool, Skeletonize (2D/3D) (49), or 3D-Sholl analysis (50). Further details can be found in *SI Appendix*.

Behavioral Analyses. The behavioral measurements were performed using the ViewPoint Zebrabox high-throughput monitoring system. Activity was recorded in separate velocity categories: inactivity (<0.5 cm/s), free-swimming (0.5–2 cm/s), and high-speed movements (>2 cm/s) (23). Data were gathered by Zebralab (ViewPoint) and analyzed with RStudio (rstudio.com). Further details can be found in *SI Appendix*.

Additional Materials and Methods. Additional information about the materials and methods, including zebrafish breeding and genotyping, immunofluorescence, ELISA, RNA extraction, cDNA synthesis, ddPCR, Western blot, statistical analyses, and experimental design can be found in *SI Appendix*.

Material and Data Availability. Manuscript and *SI Appendix* contain all data with the representative images only. The fish lines, materials, protocols, or imaging data are available upon reasonable request of the corresponding authors.

ACKNOWLEDGMENTS. We thank Kevin Ess (Vanderbilt University) for *tsc2*^{vu242}; William Harris (Cambridge University) for *SoFa1*; Michael Orger (Champalimaud Foundation) for *Tg(HuC:GCaMP5G)*; the International Institute of Molecular and Cell Biology Zebrafish Core Facility for assistance with breeding and setting up the fish; Intsol Ltd. for custom-made laboratory supplies; and Michael Arends for manuscript proofreading. This work was supported by SONATA Grant 2015/17/D/NZ3/03735 (National Science Centre, Poland) and European Commission FP7 Grant FishMed Grant Agreement No. 316125. J.Z. is a recipient of a START fellowship from the Foundation for Polish Science and a Fellowship for Extraordinary Young Scientists from the Polish Ministry of Science and Higher Education. J.J., K.K., and J.Z. were recipients of the "Mistrz" Professorial Subsidy and Fellowships; and J.J. is partly financed by the TEAM Grant POIR.04.04.00-00-5CBE/17-00, both from the Foundation for Polish Science.

1. K. R. Martin *et al*., The genomic landscape of tuberous sclerosis complex. *Nat. Commun.* **8**, 15816 (2017).
2. K. Switon, K. Kotulska, A. Janusz-Kaminska, J. Zmorzynska, J. Jaworski, Molecular neurobiology of mTOR. *Neuroscience* **341**, 112–153 (2017).
3. K. Switon, K. Kotulska, A. Janusz-Kaminska, J. Zmorzynska, J. Jaworski, Tuberous sclerosis complex: From molecular biology to novel therapeutic approaches. *IUBMB Life* **68**, 955–962 (2016).
4. P. Curatolo, R. Moavero, P. J. de Vries, Neurological and neuropsychiatric aspects of tuberous sclerosis complex. *Lancet Neurol.* **14**, 733–745 (2015).
5. A. Represa, Why malformations of cortical development cause epilepsy. *Front. Neurosci.* **13**, 250 (2019).
6. A. Mühlebner, A. Bongaarts, H. B. Sarnat, T. Scholl, E. Aronica, New insights into a spectrum of developmental malformations related to mTOR dysregulations: Challenges and perspectives. *J. Anat.* **235**, 521–542 (2019).
7. L. Meikle *et al*., A mouse model of tuberous sclerosis: Neuronal loss of Tsc1 causes dysplastic and ectopic neurons, reduced myelination, seizure activity, and limited survival. *J. Neurosci.* **27**, 5546–5558 (2007).
8. S. W. Way *et al*., Loss of Tsc2 in radial glia models the brain pathology of tuberous sclerosis complex in the mouse. *Hum. Mol. Genet.* **18**, 1252–1265 (2009).
9. K. Pollizzi *et al*., A hypomorphic allele of Tsc2 highlights the role of TSC1/TSC2 in signaling to AKT and models mild human TSC2 alleles. *Hum. Mol. Genet.* **18**, 2378–2387 (2009).
10. H. S. Bateup, K. T. Takasaki, J. L. Saulnier, C. L. Denefrio, B. L. Sabatini, Loss of Tsc1 in vivo impairs hippocampal mGluR-LTD and increases excitatory synaptic function. *J. Neurosci.* **31**, 8862–8869 (2011).
11. D. M. Feliciano, T. Su, J. Lopez, J.-C. Platel, A. Bordey, Single-cell Tsc1 knockout during corticogenesis generates tuber-like lesions and reduces seizure threshold in mice. *J. Clin. Invest.* **121**, 1596–1607 (2011).
12. R. Moavero *et al*., White matter disruption is associated with persistent seizures in tuberous sclerosis complex. *Epilepsy Behav.* **60**, 63–67 (2016).
13. L. Magri *et al*., Sustained activation of mTOR pathway in embryonic neural stem cells leads to development of tuberous sclerosis complex-associated lesions. *Cell Stem Cell* **9**, 447–462 (2011).
14. S. B. Wortmann, A. Reimer, J. W. T. Creemers, R. A. Mullaart, Prenatal diagnosis of cerebral lesions in Tuberous sclerosis complex (TSC). Case report and review of the literature. *Eur. J. Paediatr. Neurol.* **12**, 123–126 (2008).
15. M. O. Parker, A. J. Brock, R. T. Walton, C. H. Brennan, The role of zebrafish (Danio rerio) in dissecting the genetics and neural circuits of executive function. *Front. Neural Circuits* **7**, 63 (2013).
16. T. Mueller, *Atlas of Early Zebrafish Brain Development: A Tool for Molecular Neurogenetics*, T. Mueller, M. F. Wullimann, Eds. (Elsevier Science, 2005).
17. R. W. Friedrich, G. A. Jacobson, P. Zhu, Circuit neuroscience in zebrafish. *Curr. Biol.* **20**, R371–R381 (2010).
18. C. Scheldeman *et al*., mTOR-related neuropathology in mutant tsc2 zebrafish: Phenotypic, transcriptomic and pharmacological analysis. *Neurobiol. Dis.* **108**, 225–237 (2017).
19. S.-H. Kim, C. K. Speirs, L. Solnica-Krezel, K. C. Ess, Zebrafish model of tuberous sclerosis complex reveals cell-autonomous and non-cell-autonomous functions of mutant tuberin. *Dis. Model. Mech.* **4**, 255–267 (2011).
20. J. M. Peters *et al*., Loss of white matter microstructural integrity is associated with adverse neurological outcome in tuberous sclerosis complex. *Acad. Radiol.* **19**, 17–25 (2012).
21. M. L. Krishnan *et al*., Diffusion features of white matter in tuberous sclerosis with tractography. *Pediatr. Neurol.* **42**, 101–106 (2010).
22. F. M. Baumer *et al*., Corpus callosum white matter diffusivity reflects cumulative neurological comorbidity in tuberous sclerosis complex. *Cereb. Cortex* **28**, 3665–3672 (2018).
23. M. J. Winter *et al*., Validation of a larval zebrafish locomotor assay for assessing the seizure liability of early-stage development drugs. *J. Pharmacol. Toxicol. Methods* **57**, 176–187 (2008).
24. K. Wager *et al*., Neurodegeneration and epilepsy in a zebrafish model of CLN3 disease (Batten Disease). *PLoS One* **11**, e0157365 (2016).
25. D. Desmond *et al*., *Assessing Epilepsy-Related Behavioral Phenotypes in Adult Zebrafish* (Humana Press, Totowa, NJ, 2012), pp. 313–322.
26. O. Devinsky *et al*., Epilepsy. *Nat. Rev. Dis. Primers* **4**, 18024 (2018).
27. S. Jesuthasan, Fear, anxiety, and control in the zebrafish. *Dev. Neurobiol.* **72**, 395–403 (2012).
28. S. Cohen-Cory, A. H. Kidane, N. J. Shirkey, S. Marshak, Brain-derived neurotrophic factor and the development of structural neuronal connectivity. *Dev. Neurobiol.* **70**, 271–288 (2010).
29. M. Cazorla *et al*., Identification of a low-molecular weight TrkB antagonist with anxiolytic and antidepressant activity in mice. *J. Clin. Invest.* **121**, 1846–1857 (2011).
30. Z. L. Hua, F. E. Emiliani, J. Nathans, Rac1 plays an essential role in axon growth and guidance and in neuronal survival in the central and peripheral nervous systems. *Neural Dev.* **10**, 21 (2015).
31. Y. J. Choi *et al*., Tuberous sclerosis complex proteins control axon formation. *Genes Dev.* **22**, 2485–2495 (2008).
32. L. Shi, Dock protein family in brain development and neurological disease. *Commun. Integr. Biol.* **6**, e26839 (2013).
33. B. D. Fontana, N. J. Mezzomo, A. V. Kalueff, D. B. Rosemberg, The developing utility of zebrafish models of neurological and neuropsychiatric disorders: A critical review. *Exp. Neurol.* **299**, 157–171 (2018).
34. A. V. Kalueff *et al*.; Zebrafish Neuroscience Research Consortium, Towards a comprehensive catalog of zebrafish behavior 1.0 and beyond. *Zebrafish* **10**, 70–86 (2013).
35. S. Molas, S. R. DeGroot, R. Zhao-Shea, A. R. Tapper, Anxiety and nicotine dependence: Emerging role of the habenulo-interpeduncular axis. *Trends Pharmacol. Sci.* **38**, 169–180 (2017).
36. H. Aizawa, R. Amo, H. Okamoto, Phylogeny and ontogeny of the habenular structure. *Front. Neurosci.* **5**, 138 (2011).
37. O. Hikosaka, The habenula: From stress evasion to value-based decision-making. *Nat. Rev. Neurosci.* **11**, 503–513 (2010).

38. B. B. Zhang, Y. Y. Yao, H. F. Zhang, K. Kawakami, J. L. Du, Left habenula mediates light-preference behavior in zebrafish via an asymmetrical visual pathway. *Neuron* **93**, 914–928 (2017).
39. R. M. Colwill, R. Creton, Imaging escape and avoidance behavior in zebrafish larvae. *Rev. Neurosci.* **22**, 63–73 (2011).
40. F. Liu *et al*., Effectiveness of low dose of rapamycin in preventing seizure-induced anxiety-like behavior, cognitive impairment and defects in neurogenesis in developing rats. *Int. J. Neurosci.* (2018).
41. M. Lopez de Armentia *et al*., cAMP response element-binding protein-mediated gene expression increases the intrinsic excitability of CA1 pyramidal neurons. *J. Neurosci.* **27**, 13909–13918 (2007).
42. A. Das, M. Dines, J. M. Alapin, R. Lamprecht, Affecting long-term fear memory formation through optical control of Rac1 GTPase and PAK activity in lateral amygdala. *Sci. Rep.* **7**, 13930 (2017).
43. L. Chen *et al*., Rac1 controls the formation of midline commissures and the competency of tangential migration in ventral telencephalic neurons. *J. Neurosci.* **27**, 3884–3893 (2007).
44. H. Kassai *et al*., Rac1 in cortical projection neurons is selectively required for midline crossing of commissural axonal formation. *Eur. J. Neurosci.* **28**, 257–267 (2008).
45. N. G. Hedrick *et al*., Rho GTPase complementation underlies BDNF-dependent homo- and heterosynaptic plasticity. *Nature* **538**, 104–108 (2016).
46. Y. Miyamoto, J. Yamauchi, A. Tanoue, C. Wu, W. C. Mobley, TrkB binds and tyrosine-phosphorylates Tiam1, leading to activation of Rac1 and induction of changes in cellular morphology. *Proc. Natl. Acad. Sci. U.S.A.* **103**, 10444–10449 (2006).
47. V. Zamboni *et al*., Disruption of ArhGAP15 results in hyperactive Rac1, affects the architecture and function of hippocampal inhibitory neurons and causes cognitive deficits. *Sci. Rep.* **6**, 34877 (2016).
48. J. Schindelin *et al*., Fiji: An open-source platform for biological-image analysis. *Nat. Methods* **9**, 676–682 (2012).
49. T. C. Lee, R. L. Kashyap, C. N. Chu, Building skeleton models via 3-D medial surface axis thinning algorithms. *CVGIP Graph. Models Image Process.* **56**, 462–478 (2002).
50. T. A. Ferreira *et al*., Neuronal morphometry directly from bitmap images. *Nat. Methods* **11**, 982–984 (2014).